Permanent Magnetism in Dithiol-Capped Silver Nanoparticles

Lorenza Suber,* Dino Fiorani, Guido Scavia, and Patrizia Imperatori

CNR-Istituto Struttura della Materia, P.O. Box 10, 00016 Monterotondo St., Italy

William R. Plunkett

Center for Advanced Materials Processing, Clarkson University, Potsdam, New York 13699-5814

Received September 4, 2006. Revised Manuscript Received December 31, 2006

Silver nanoparticles, capped with oleic acid, with mean diameters varying between 2.8 and 5.7 nm, have been synthesized by the polyol method and 1,6-hexane dithiol was subsequently substituted for the oleic acid. Whereas oleic acid-capped silver nanoparticles, like bulk silver, show a diamagnetic behavior, dithiol-capped silver nanoparticles exhibit a permanent magnetism, with a finite coercivity, up to room temperature. The permanent magnetism is associated with blocked, highly anisotropic localized magnetic moments at the particle surface, due to the spins of 4d localized holes generated through Ag−S bonds. The strong anisotropy is a result of the combination of spin−orbit coupling and the breaking of lattice symmetry of surface particle Ag atoms involved in both Ag−Ag and Ag−S bonds.

Introduction

The magnetic properties of nanoparticles are the focus of increasing interest for the basic understanding of magnetism, as they represent very good model systems, and for their applications in a wide range of fields, e.g., high-density data storage,[1] ferrofluid technology,[2] nanobiotechnology,[3] and biomedicine.[4]

Size confinement to a nanometer scale can induce completely different magnetic properties with respect to the corresponding bulk material with the same chemical composition, but structured on a micrometer length scale. The surface electronic structure plays a dominant role in tuning the magnetic properties, especially for very small particles, below about 5 nm, due to the very high percentage of atoms located at the particle surface. The surface is characterized by disorder, due to missing bonds and local variation of the number of atomic neighbors, and a reduction of lattice symmetry with respect to the core of the particle.[5]

It has recently been reported that surface bonds with suitable ligands can induce a permanent magnetism, even in nanoparticles of nonmagnetic materials, if they are small enough.[6a−d] The nanosize effect may result in stronger d−d interactions, due to lattice contraction and the decrease of interatomic distances, so that the d holes decrease at the metal surface atoms with respect to those in the bulk.[7a] On the other hand, interaction of the surface atoms with capping agents can produce the opposite effect.[7b] Actually, the combined control of particle size and the surface environment allows tuning of the electronic structure of the metal particles through the optimization of surface energy and metal adsorbate interaction, thus strongly modifying their properties. As a matter of fact, while gold is diamagnetic and palladium is paramagnetic as bulk materials, permanent magnetism has been observed in gold and palladium nanoparticles, exhibiting hysteresis cycles up to room temperature, when capped by thiols.[6b,8] This behavior can be explained by localized magnetic moments originating from 5d(4d) holes through Au(Pd)−S bonds. They result in a high magnetic anisotropy due to the combination of high spin−orbit coupling and symmetry reduction because of the coexistence of two types of bonds, Au(Pd)−Au(Pd) and Au(Pd)−S. As a matter of fact, adsorbed thiolate layers on gold thin films induce magnetic behavior as well.[9a−b]

In this context, we have investigated the magnetic behavior of nanometer-sized silver nanoparticles capped with 1,6-hexanedithiol.

The bidentate dithiol ligand, instead of the monodentate thiol, has been chosen for possible application of the material in the form of thin particle layers anchored through an S− bond to a substrate.[10] Silver, among all metals, is receiving special attention since it has the highest thermal and electrical

* Corresponding author. E-mail: lorenza.suber@ism.cnr.it.

(1) Mallinson, J. C. *The Foundations of Magnetic Recording*; Academic: Berkeley, 1987; Chapter 3.
(2) Raj, K.; Moskowitz, R. *J. Magn. Magn. Mater.* **1999**, *85*, 233.
(3) Niemeyer, C. M. *Curr. Opin. Chem. Biol.* **2000**, *4*, 609.
(4) Häfeli, U.; Schütt, W.; Teller, J.; Zborowski, M. *Scientific and Clinical Applications of Magnetic Carriers*; Plenum Press: New York, 1977.
(5) *Surface Effects in Magnetic Nanoparticles*; Fiorani, D., Ed.; Springer-Verlag: New York, 2004.
(6) (a) Hori, H.; Teranishi, T.; Nakae, Y.; Seino, Y.; Miyake, M.; Yamada, S. *Phys. Lett. A* **1999**, *263*, 406. (b) Crespo, P.; Litrán, R.; Rojas, T. C.; Multigner, M.; de La Fuente, J. M.; Sánchez López, J. C.; García, M. A.; Hernando, A.; Penadés, S.; Fernández, A. *Phys. Rev. Lett.* **2004**, *93*, 087204. (c) Hernando, A.; Sampredo, B.; Litrán, R.; Rojas, T. C.; Sánchez López, J. C.; Fernández, A. *Nanotechnology* **2006**, *17*, 1449. (d) Yamamoto, Y.; Miura, T.; Suzuki, M.; Kawamura, N.; Miyagawa, H.; Nakamura, T.; Kobayashi, K.; Teranishi, T.; Hori, H. *Phys. Rev. Lett*. **2004**, *93*, 11680.
(7) (a) Zhang, P.; Sham, T. K. *Phys. Rev. Lett.* **2003**, *90*, 245502. (b) Zhang, P.; Sham, T. K. *Appl. Phys. Lett.* **2002**, *81*, 736.
(8) Litrán, R.; Sampredo, B.; Rojas, T. C.; Multigner, M.; Sánchez López, J. C.; Crespo P.; López-Cartes, C.; García, M. A.; Hernando, A.; Fernández, A. *Phys. Rev. B* **2006**, *73*, 054404.
(9) (a) Hernando, A.; Crespo, P.; García, M. A. *Phys. Rev. Lett*. **2006**, *96*, 057206. (b) Vager, Z.; Carmeli, I.; Leitus, G.; Reich, S.; Naaman, R. *J. Phys. Chem. Solids* **2004**, *65*, 713 and refs therein.

10.1021/cm062093a CCC: $37.00
Published on Web 02/24/2007

conductivities. With regard to its magnetic behavior, however, bulk silver is diamagnetic with a susceptibility $\chi = -1.8 \times 10^{-7}$ emu/g Oe. Ferromagnetism occurs basically because of the spatial localization of the d orbitals near the top of a d band. This localization produces both a large density of states near the Fermi level ($N(E_f)$) (when the band is nearly full) and a relative maximum in the exchange−correlation integral I.[11] For Ag ($4d^{10}s^1$) with an fcc structure, however, the d bands are far from E_f (about 2 eV) and analysis of the bands intersecting the E_f reveals that the states at E_f are mainly s states with some p contribution.[12,13]

The results of magnetization measurements of dithiol-capped silver nanoparticles provided evidence of the existence of permanent magnetism up to room temperature, as shown by hysteresis cycles with finite coercivity, whereas diamagnetic behavior was observed for the corresponding oleic acid-capped Ag nanoparticles.

Experimental Procedures

Materials and Synthesis Procedures. The reagents silver acetyl acetonate ($C_5H_8O_2$)Ag, 1,2-hexadecanediol ($CH_3(CH_2)_{13}CH(OH)$-CH_2OH, oleic acid ($CH_3(CH_2)_7CH{=}CH(CH_2)_7COOH$), oleyl amine ($CH_3(CH_2)_7CH{=}CH(CH_2)_8(NH_2)$, 1,6-hexanedithiol ($HS(CH_2)_6SH$), dibenzyl ether 99%, *n*-hexane, and ethyl alcohol anydrous were purchased from Aldrich and used as-received.

Synthesis of Monodispersed Silver Nanoparticles. The preparation method employed was introduced by Sun et al. for the synthesis of monodispersed ferrite nanoparticles.[14,15] It consists of chemical reduction of metallorganic compounds by polyols in solution, at high temperatures. To obtain silver particles of different mean diameters, changes in the reaction procedure were introduced.

Silver Nanoparticles (S01) with $\langle d \rangle = 2.8$ nm. 1,2-Hexadecanediol (1.44 g, 5 mmol) was heated to 200 °C in an oil bath under stirring and a flux of nitrogen. A solution of silver acetyl acetonate (207 mg, 1 mmol), oleic acid (1.42 mL, 4 mmol), and oleyl amine (1.9 mL, 4 mmol) in 10 mL of dibenzyl ether was rapidly added. After 20 min, the temperature was rapidly raised to 240 °C and the reaction stirred for 30 min. The oil bath was then removed and the flask rapidly cooled to r.t. by its immersion in a cool water bath. By addition of ethyl alcohol (10 mL) to the reaction suspension, a brown precipitate was formed. It was then centrifuged at 4000 rpm for 10 min and the precipitate separated from the liquor. The precipitate was suspended in a solution of ∼0.05 mL of oleic acid and ∼0.05 mL of oleyl amine in 30 mL of *n*-hexane and then centrifuged to eliminate the product from insoluble impurities. Ethyl alcohol (30 mL) was then added to the suspension and the mixture was centrifuged. The precipitate was once again dissolved in *n*-hexane, precipitated with ethyl alcohol and centrifuged. Finally, it was dried under vacuum overnight.

Silver Nanoparticles (S02) with $\langle d \rangle = 4$ nm. The flask was heated in an oil bath to 170 °C. 1,2-Hexadecanediol (1.44 g, 5 mmol), dissolved in 8 mL of dibenzyl ether, was added, and under magnetic stirring and a flux of nitrogen, a solution of silver acetyl acetonate (207 mg, 1 mmol), oleic acid (1.42 mL, 4 mmol), and oleyl amine (1.9 mL, 4 mmol) in 2 mL of dibenzyl ether was added. The temperature was rapidly raised to 200 °C. After 20 min, the oil bath was removed and the reaction flask was rapidly cooled to r.t. The treatment was then the same as the one used above. Analysis: C, 12.57%; H, 1.84%. H/C atomic ratio = 1.74 (H/C atomic ratio for oleic acid = 1.83).

Silver Nanoparticles (S03) with $\langle d \rangle = 5.7$ nm. 1,2-Hexadecanediol (1.44 g, 5 mmol) was dissolved in 8 mL of dibenzyl ether and, under magnetic stirring, heated to 200 °C in an oil bath. A solution of silver acetyl acetonate (207 mg, 1 mmol), oleic acid (1.42 mL, 4 mmol), and oleyl amine (1.9 mL, 4 mmol) in 2 mL of dibenzyl ether was rapidly added. The temperature was raised to 240 °C. After 20 min the oil bath was removed and the flask was rapidly cooled to r.t. The treatment was then the same as the one used for S01.

Silver Nanoparticles (S1, S2, S3) Capped with 1,6-Hexanedithiol. S01, S02, and S03 silver nanoparticles were dissolved in 200 mL of *n*-hexane, forming a reddish brown suspension. A solution of 1,6-hexanedithiol (0.6 mL, 3.77 mmol) in 250 mL of *n*-hexane was added in 30 min, whereby a precipitate was formed. The precipitate was centrifuged and washed three times; each time the powder was dissolved in ethyl alcohol and precipitated by addition of *n*-hexane. The products were then dried under vacuum.

Analyses. S1: C, 6.30%; H, 0.89%; S, 4.23%. S2: C, 4.29%; H, 0.60%; S, 2.26%. S3: C, 3.89%; H, 0.65%; S, 3.40%. C/H/S: 6/12/2. Theoretical C/H/S for 1,6-hexanedithiol: 6/12/2.

ICP-MS analyses of samples S1−S3 showed impurities of Ni, Co, and Fe to be below about 20, 30, and 70 ppm, respectively.

Physical Techniques. Elemental analyses (C, H, N, S) were performed by Laboratorio Microanalisi, Area della Ricerca Roma1, Monterotondo (Italy) and Ni, Co, and Fe impurities were determined with an inductively coupled plasma mass spectrometer (ICP-MS) by Malissa Laboratories (Germany).

UV−visible absorption measurements were performed with a UV−vis−NIR Cary 5 spectrophotometer.

Powder X-ray diffraction (XRD) measurements were carried out in the 2θ range 25−80° by means of an automated Seifert powder diffractometer using Cu Kα radiation (1.5418 Å).

Transmission electron microscopy (TEM) and X-ray elemental analysis were performed with a JEOL 2010 TEM/STEM (scanning transmission electron microscope), equipped with an Oxford Instruments "Inca" EDS (energy dispersive spectrometer) system, at an accelerating voltage of 200 kV.

Scanning tunneling microscopy (STM) measurements were carried out with a commercial STM-UHV system (WA tech.). The typical tunneling parameters are tip−sample voltage = 2−3 V and tunneling current = 0.05−0.08 nA. The mean particle diameter ($\langle d \rangle$) was determined by STM analysis by measuring about 100 particle diameters for each sample.

Magnetic measurements were carried out on a commercial SQUID (superconducting quantum interference device) magnetometer operating between 2 and 400 K, with a maximum magnetic field of 55 kOe. The samples were measured as powders, slightly compacted inside the sample holder. The diamagnetic contribution of the sample holder, Ag particle core, and 1,6-hexanedithiol have been subtracted from the experimental magnetization.

Results and Discussion

Silver nanoparticles with a narrow size distribution were obtained by reaction at high temperatures of a solution of silver acetyl acetonate and surfactants with 1,2-hexade-

(10) Colvin, V. L.; Alivisatos, A. L.; Tobin, J. G. *Phys. Rev. Lett.* **1991**, *66*, 2786.
(11) Janak, J. F. *Phys. Rev. B* **1977**, *16*, 255.
(12) Drube, W.; Sham, T. K.; Kravisova, A.; Soldatov, A. V. *Phys. Rev. B* **2003**, *67*, 035122.
(13) Nautiyal, T; Youn, S. J.; Kim, K. S. *Phys. Rev. B.* **2003**, *68*, 033407.
(14) Sun, S.; Zeng, H.; Robinson, B. D.; Raoux, S.; Rice, P. M.; Wang, X. S.; Li, G. *J. Am. Chem. Soc.* **2004**, *126*, 273.
(15) Cattaruzza, F.; Fiorani, D.; Flamini, A.; Imperatori, P.; Scavia, G.; Suber, L.; Testa, A. M.; Mezzi, A.; Ausanio, G.; Plunkett, W. R. *Chem. Mater.* **2005**, *17*, 3311.

canediol (polyol). After the nucleation process, the temperature was raised further to favor the crystallization process. The silver particles *as-prepared* were capped by the surfactant oleic acid to avoid particle−particle aggregation. Then, oleic acid was exchanged with the stronger ligand 1,6-hexanedithiol. The two-step process, i.e., using first, as surfactant, oleic acid and then exchanging it at room temperature with the dithiol, was necessary because of the thermal instability of the dithiol ligand at the high reaction temperatures. This two-step procedure, however, probably has as a side effect, an incomplete dithiol particle covering.

Three different samples of silver nanoparticles capped with 1,6-hexanedithiol, S1, S2, and S3, have been characterized. To tailor the particle size in samples S02 and S03, temperatures have been varied, higher for S03 than for S02. The effect is an increase in particle size with increasing temperature, also observed by Sun et al.[14] Besides favoring the crystallization process, the higher temperatures probably contribute to enhanced particle growth. Moreover, in the case of S01, the polyol concentration has been changed, adding the solution of silver acetyl acetonate and surfactants to the *pure* polyol, instead of to a polyol solution. In this way, the silver acetyl acetonate first comes in contact with a high concentration of the polyol reducing agent. This probably results in a decrease in particle size.

S1 consists of the smallest silver particles ($\langle d \rangle = 2.8$ nm). Based on elemental analyses (see the Experimental Section) and considering that 44% of the silver atoms lies on the particle surface,[16] the ratio between silver atoms on the surface and dithiol molecules is 5.5.

S2 is constituted by silver particles with $\langle d \rangle = 4$ nm. Based on elemental analyses and considering that 26% of the silver atoms lies on the particle surface, the ratio between Ag atoms on the surface and dithiol molecules is 6.3.

S3 is constituted by silver particles with $\langle d \rangle = 5.7$ nm. Based on elemental analyses and considering that 13% of the silver atoms lies on the particle surface, the ratio between silver atoms on the surface and dithiol molecules is 2.1.

Structural, Morphological, and Optical Characterization. Figure 1 shows the X-ray diffraction pattern of S02 silver particles. The peaks are indexed according to the fcc silver structure (4-783 JPCDS-ICDD). The lattice parameter calculated from the 2θ peak positions, through a least-square refinement procedure, is 4.079 ± 0.021 Å. The peak broadening can mainly be attributed to the small crystallite size. An average size of 3.8 nm was estimated from the half-width of the reflections, using the Scherrer equation.[17]

Figures 2a and 2b show an STM micrograph and size distribution of S01 silver particles before being capped by dithiol and Figures 3a−3c and Figures 4a and 4b show micrographs and size distribution of dithiol-capped silver particles. According to the histogram of Figure 2b, the dimensions of the S01 silver particles peak at 2.8 nm. The right tail of the histogram could be attributed to the effect of some particle agglomeration. Silver particles capped by dithiol (S1) are shown in Figures 3a and 3b. Figure 3a reveals that the clusterization process, favored by the bidentate ligand dithiol, gives rise to elongated structures oriented along a preferential direction. A higher magnification of the clusters (Figure 3b) shows a coexistence of particles with typical diameters of 5 and 2 nm, probably corresponding to the coated and uncoated particles, respectively. This is also evident in the histogram of Figure 3c, where the two maxima at 5 and 2 nm appear.

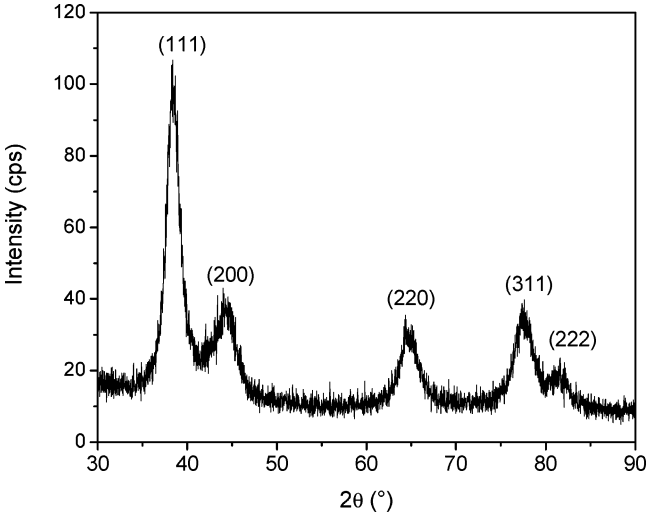

Figure 1. X-ray diffraction pattern of S02 silver particles.

The S2 particle distribution is spread between 2 and 5 nm and their shape is more elongated compared to the corresponding uncoated silver particles (figures not shown).

Finally, Figures 4a and 4b show the S3 sample constituted by bigger particles and agglomerates with diameters up to 30 nm.

As an example, typical TEM micrographs of the oleic acid-capped and dithiol-capped silver particles are shown in Figures 5a and 5b. The bigger spots in Figure 5a are formed by more than one particle. One should note the tendency, as evidenced also by STM analyses, of the bidentate dithiol ligand to align and connect the silver particles.

Preliminary S 2p XPS measurements of the silver particles coated with dithiol[18] showed a peak with a maximum at 162.3 eV. From published data,[19] the peak can be attributed to sulfur atoms strongly bound to silver atoms. The proximity of sulfur to silver is further confirmed by TEM and EDS analyses of S1. By comparing Figure 6b and Figure 6c, which map the elements sulfur and silver, it can be observed, in fact, that all the sulfur is found in the proximity of the silver atoms, whereas the halo visible in Figure 6a is due to silica impurities (Figure 6d).

XANES (X-ray absorption near-edge spectroscopy) measurements at the sulfur K edge also evidenced the coordination of sulfur to silver.[20]

(16) The number of particle surface Ag atoms was calculated as follows: particle surface/crystal cell surface = number of crystal cells per particle surface; number of cells × number of Ag atoms per cell = number of particle surface Ag atoms. The % was then established on the basis of the total particle Ag atoms. They were calculated in the same way as for the surface Ag atoms, but considering the particle Ag volume and the Ag cell volume.

(17) Klug H. P.; Alexander L. E. *X-Ray Diffraction Procedures for Polycrystalline and Amorphous Materials*; Wiley: New York, 1967.

(18) Mezzi, A. Private communication.

(19) Castner, D. G.; Hinds, K.; Grainger, D. W. *Langmuir* **1996**, *12*, 5083.

(20) Mobilio, S. Private communication.

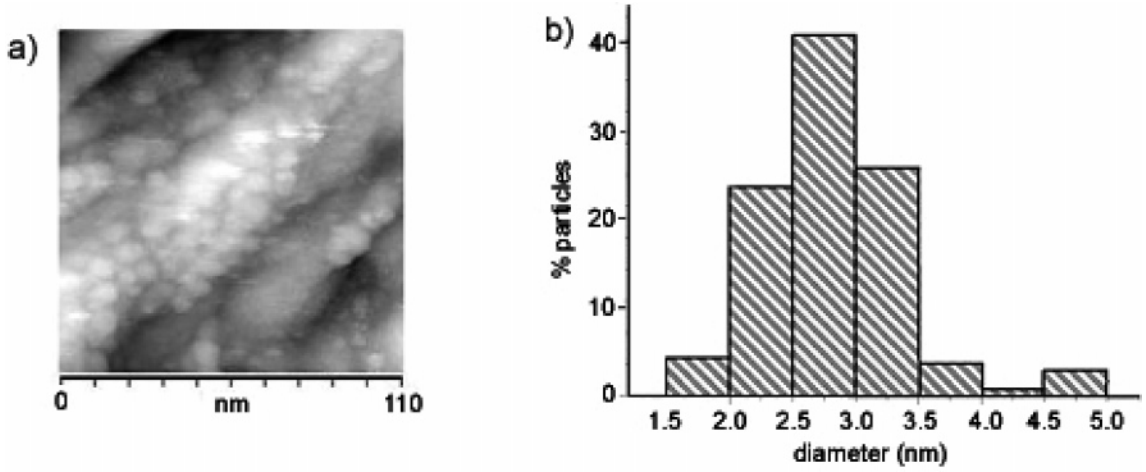

Figure 2. (a) STM image of S01 silver particles covered by oleic acid onto the Au substrate. (b) Corresponding histogram of the size distribution ($\langle d \rangle$ = 2.8 nm; σ = 0.4 nm).

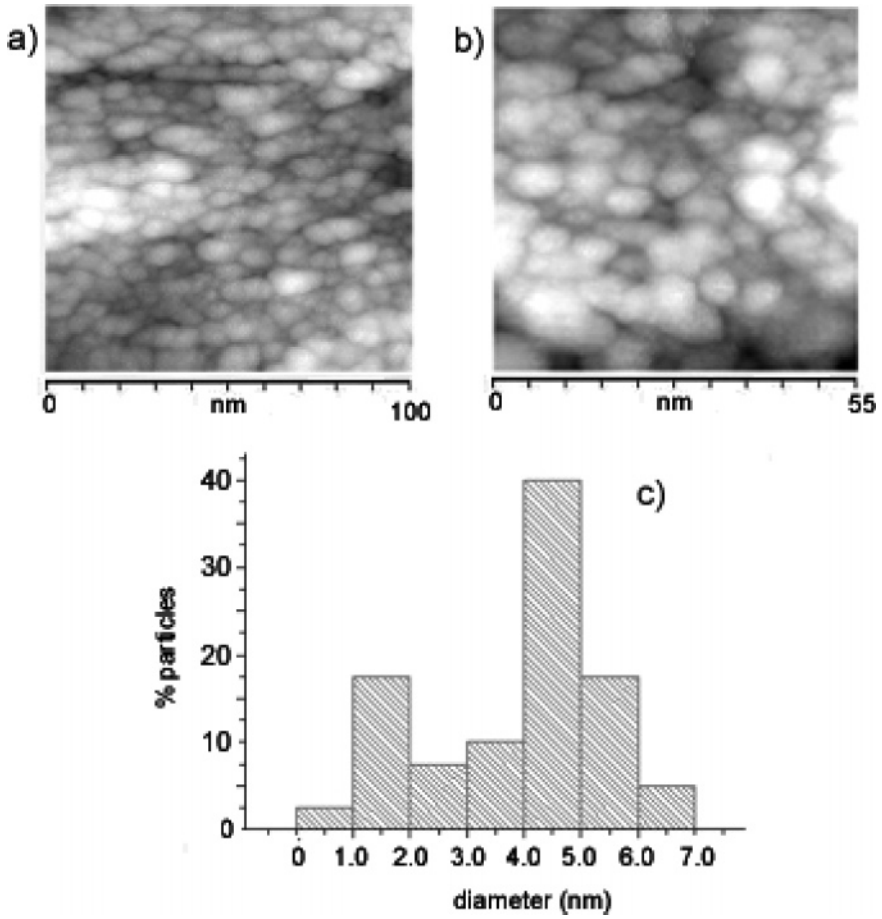

Figure 3. (a)−(b) STM images of S1 silver particles capped by dithiol at different magnifications. (c) Corresponding histogram of the size distribution.

UV−visible measurements of silver particles not capped by dithiol show an absorption band with a maximum at 414 nm (Figure 7a). This band is associated with the so-called surface plasmon resonance which corresponds to a collective oscillation of electrons on the particle surface.[21] The position of the maximum depends on the particle size and shape and on the dielectric constant of the dispersant.[22] The shape of the measured absorption curve is characteristic of monodispersed nanoparticles without interparticle effects.

UV−visible measurements of silver particles capped by dithiol show, in all cases, a broad absorption with a maximum at about 600 nm and a shoulder at about 410 nm (Figure 7b). The appearance of a maximum at 600 nm (besides the shoulder at 400 nm, which can be attributed to a fraction of silver atoms not capped by dithiols; see STM analyses above) is quite different from the optical spectra of *thiol*-coated silver particles. For silver particles coated with thiols, in fact, the position of the absorption maximum does not change

(21) Creighton, J. A.; Eadon, D. G. *J. Chem. Soc., Faraday Trans.* **1991**, *87*, 3881.
(22) Gaikward, A. V.; Verschuren, P.; Eiser, E.; Rothenberg, G. *J. Phys. Chem. B* **2006**, *110*, 17437.

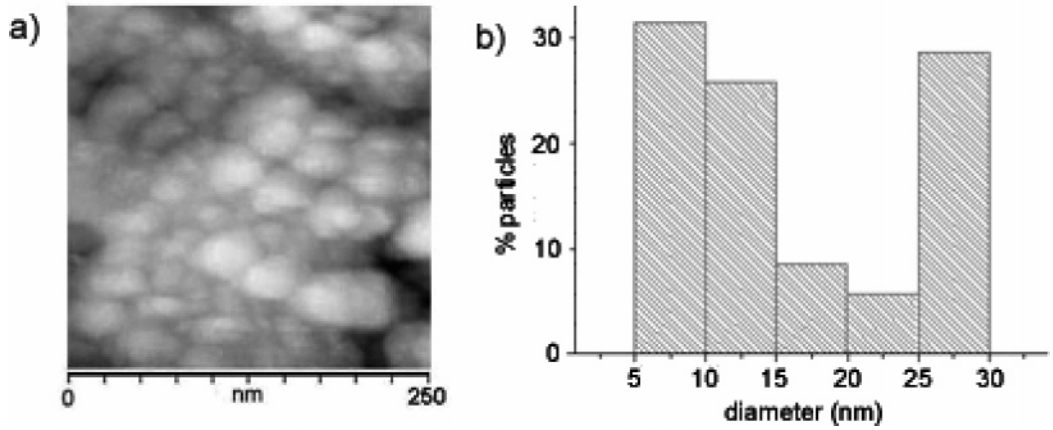

Figure 4. (a)−(b) STM images of the S3 particle aggregates covered by dithiol at different magnifications. (c) Corresponding histogram of the size distribution.

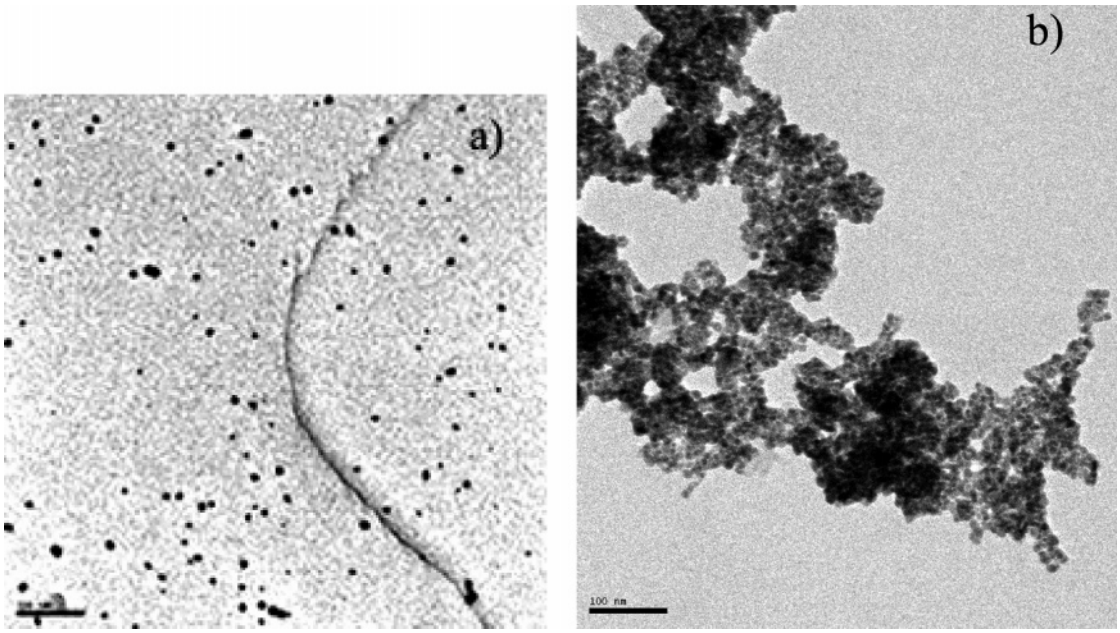

Figure 5. (a) TEM micrograph of S02 oleic acid-capped silver particles (scale bar = 100 nm). (b) TEM micrograph of S2 dithiol-capped silver particles (scale bar = 100 nm).

remarkably.[23] The shift of the maximum observed in all dithiol-capped silver samples could be due to particle−particle aggregation, caused by the bidentate dithiol ligand, evident from comparison of the TEM micrographs in Figures 5a and 5b of the oleic acid-capped and dithiol-capped particles. The effect of the broadening of the band and a decreased intensity can be explained, according to Henglein,[24] considering an increasing of ϵ_2 (the imaginary part of the dielectric constant of silver) by the capped dithiol. Since ϵ_2 increases with decreasing lifetime of the plasmon oscillation, this implies that the dithiol shortens the lifetime of the plasma oscillation, probably by coupling of the plasmons with the phonons in the dithiol. Finally, it should be noted that the presence of the plasmon resonance absorption band at 600 nm suggests that silver particles exhibit surface metallic conductivity even when the particle is capped by the dithiol molecules.

Magnetic Characterization. Magnetization measurements were performed, as a function of the magnetic field and temperature, on oleic acid- and 1,6-hexanedithiol-capped Ag particles. The *M* vs *T* measurements were performed according to the zero-field-cooling (ZFC) and field-cooling (FC) procedures. ZFC curves were obtained as follows: first, the sample is cooled in zero magnetic field from 300 to 5 K; the magnetic field is then applied and the magnetization is measured while increasing the temperature. FC curves are subsequently obtained by measuring the magnetization while the temperature is decreased from 300 to 5 K in the same magnetic field.

Oleic Acid-Capped Silver Particles. The results of ZFC/FC magnetization measurements for the sample S03 are reported in Figure 8. A diamagnetic behavior is shown, as observed in bulk silver. However, below about 100 K, a weak paramagnetic contribution is observed, likely due to a very small fraction of free spins probably coming from some impurities. Correspondingly, *M* vs *H* measurements show paramagnetic-like behavior at 5 K and a diamagnetic one at 100 and 300 K (Figure 9). The same kind of behavior was observed for sample S02.

(23) Suber, L. Unpublished results.
(24) Henglein, A. *J. Phys. Chem.* **1993**, *97*, 5457.

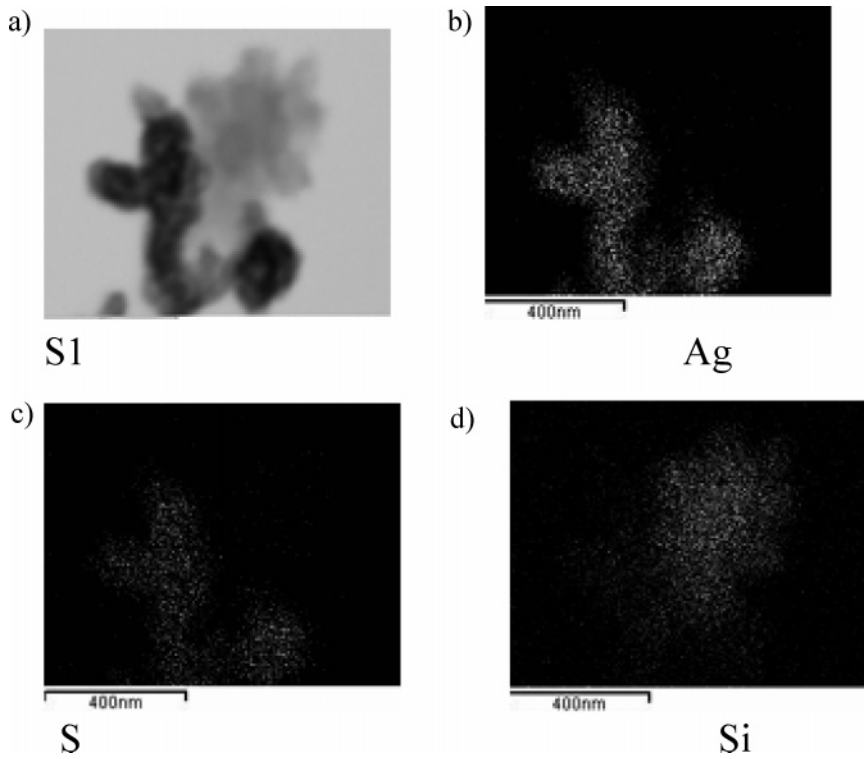

Figure 6. (a) TEM micrograph of S1 dithiol-capped silver particles. (b) EDS X-ray map of silver atoms. (c) EDS X-ray map of sulfur atoms. (d) EDS X-ray map of silicon atoms.

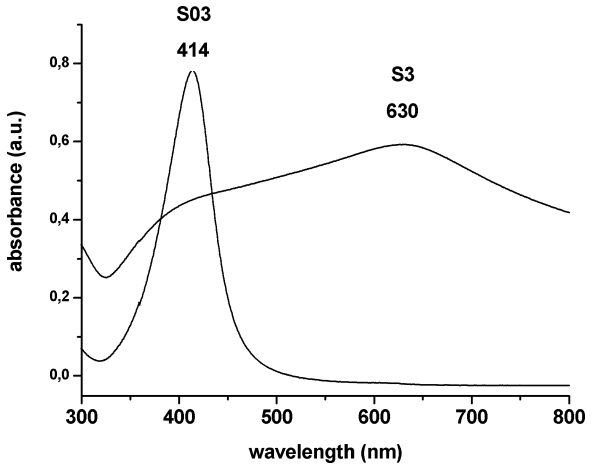

Figure 7. UV−visible absorption of silver particles (S03) and dithiol-capped silver particles (S3).

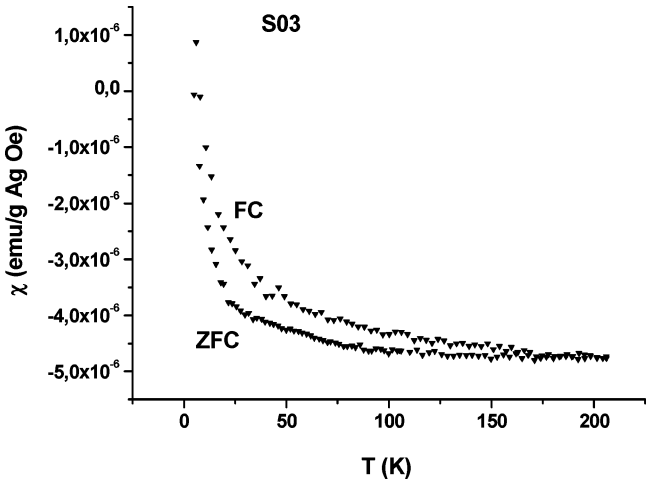

Figure 8. Magnetic susceptibility (ZFC/FC) of S03 oleic acid-capped silver particles (H = 200 Oe).

Dithiol-Capped Silver Particles. *S1*. The ZFC magnetization (Figure 10) shows a maximum at T_{max} = 13 K, whereas the FC branch continues to increase with decreasing temperature in a Curie−Weiss-type behavior. The branching of the two curves occurs at high temperature, not visible at the scale of the figure. This is consistent with saturating hysteresis loops at 100 and 300 K (Figure 11), confirming that a fraction of the moments are still blocked at room temperature. The coercive fields (H_c) are quite low: H_c = 50 Oe at 100 K; H_c = 13 Oe at 300 K. The hysteresis loop at 5 K (Figure 11) shows two contributions: a ferromagnetic like one, tending to saturate, which determines the rapid increase of magnetization in the low field region, and a paramagnetic one, responsible for the linear behavior in the high field region. The first contribution is due to the blocked moments, responsible for the observed coercivity (H_c = 70 Oe), whereas the second is due to the paramagnetic impurities, as observed in the uncapped particles.

S2. The ZFC curve (Figure 12) shows a broad maximum between 100 and 200 K, whereas the FC curve increases continuously with decreasing temperature, deviating from the ZFC curve below about 320 K. This behavior, qualitatively similar to the blocking process of magnetic nanoparticle moments, reveals the presence of a large distribution of magnetic anisotropy. It gives rise to a distribution of blocking temperatures T_b, the temperature at which, for a defined measuring time, the effective anisotropy energy for each particle moment becomes equal to the thermal energy. Hysteresis loops are observed up to room temperature (Figure 13), with the saturation magnetization values not changing significantly with temperature. The coercivity values are as follows: H_c = 210 Oe at 5 K; H_c = 80 Oe at 100 K; H_c =

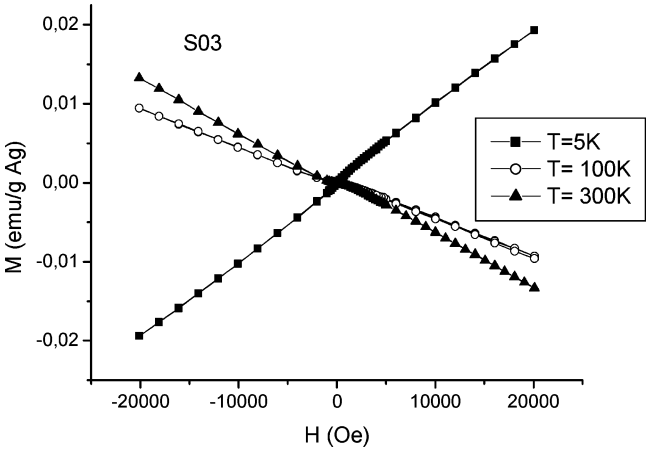

Figure 9. Hysteresis loops at different temperatures of S03 oleic acid-capped silver particles.

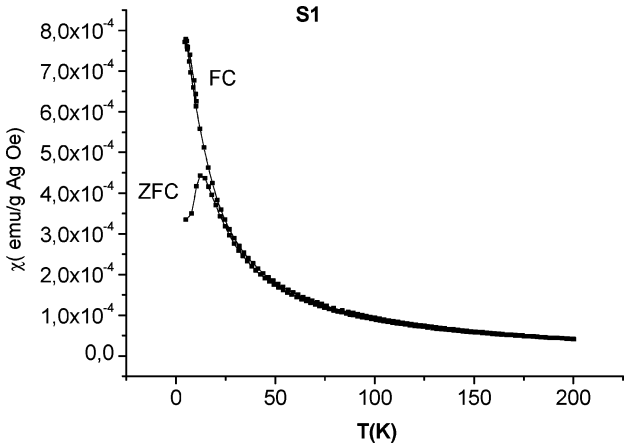

Figure 10. Magnetic susceptibility (ZFC/FC) of S1 dithiol-capped silver particles (H = 10 Oe).

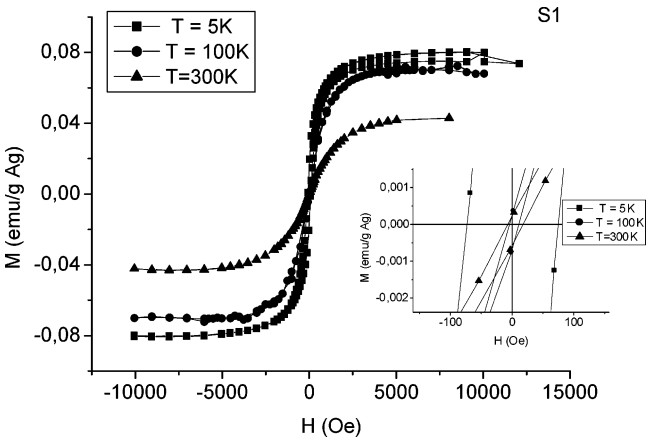

Figure 11. Hysteresis loops at different temperatures of S1 silver dithiol-capped particles. The inset shows a more detailed view of the thermal coercivity response.

60 Oe at 300 K. The weak temperature dependence of both M_s (saturation magnetization) and H_c suggests that there are blocked moments up to temperatures higher than 300 K, i.e., with blocking temperatures higher than 300 K. The magnetic moment for the silver atom, deduced from the saturation magnetization at 5 K, is 0.008 μ_B, taking 2105 as the total number of silver atoms per particle and 26% of them as being at the particle surface.

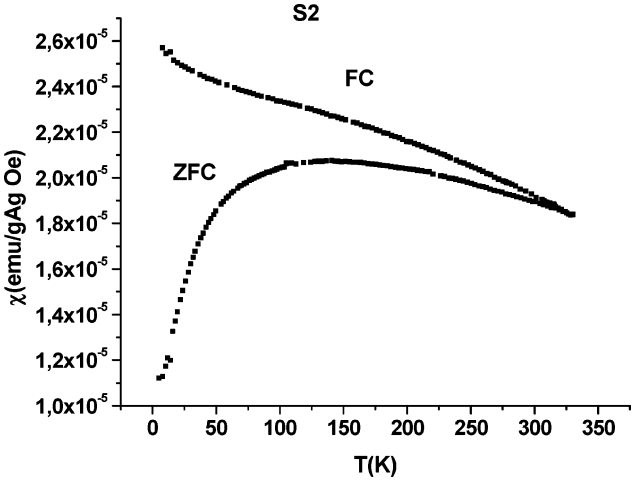

Figure 12. Magnetic susceptibility (ZFC/FC) of S2 dithiol-capped silver particles (H = 200 Oe).

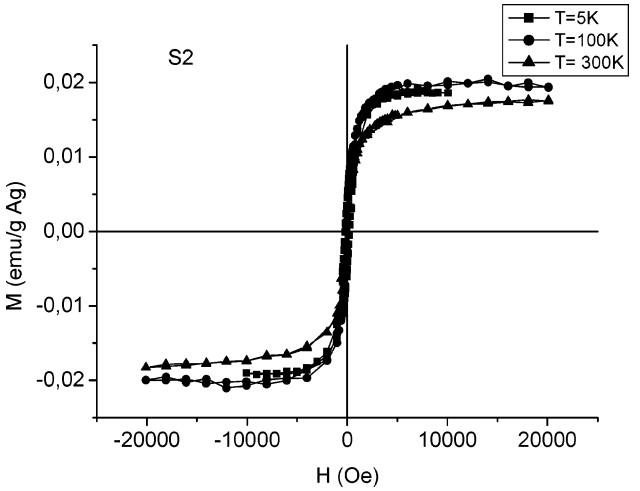

Figure 13. Hysteresis loops at different temperatures of S2 dithiol-capped silver particles.

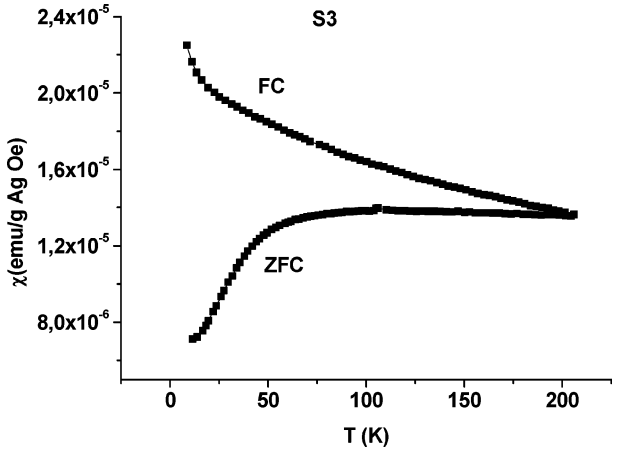

Figure 14. Magnetic susceptibility (ZFC/FC) of S3 dithiol-capped silver particles (H = 200 Oe).

S3. The ZFC curve shows, with increasing temperature, an increase of magnetization up to 80 K, where it reaches a temperature-independent value up to 300 K (Figure 14). This indicates that the anisotropy energies are shifted to higher values with respect to those of sample S2. This is understandable, considering that, in this sample, a larger fraction of silver surface atoms are involved in the S bonding with

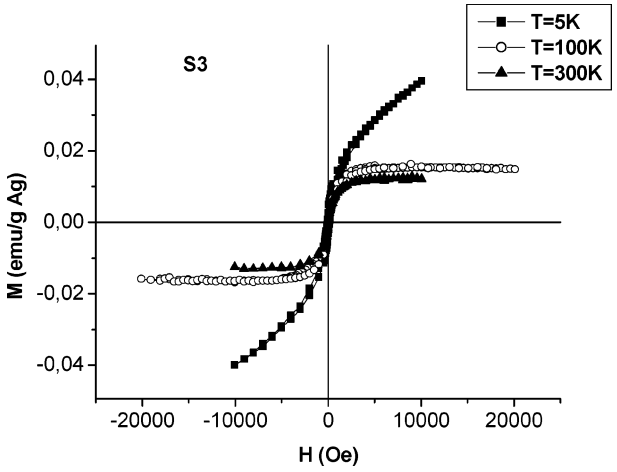

Figure 15. Hysteresis loops at different temperatures of S3 dithiol-capped silver particles.

respect to the silver surface atoms of sample S2. In the case of sample S3, in fact, the ratio (surface silver atoms)/dithiol, deduced from elemental analyses, is 2.1, whereas for the S2 sample, the ratio is 6.3, implying that a larger fraction of Ag atoms are uncapped.

Finally, the smaller coercivities with respect to the S2 sample, H_c =115 Oe at 5 K, H_c = 89 Oe at 100 K, and H_c =16 Oe at 300 K (Figure 15), should be related to the presence of bigger particles and aggregated as observed by STM measurements.

The possibility that the observed magnetic moments are due to the magnetic impurities of Co, Ni, and Fe is ruled out since they should be in the metallic bulk state to give comparable magnetic moments. The impurities are, instead, due to the chemical preparation method, in the oxidized antiferromagnetic state (CoO, NiO, and α-Fe_2O_3 with a weak ferromagnetism above the Morin temperature (T_M = 265 K) and in the form of very small particles exhibiting a superparamagnetic behavior at room temperature.

The origin of the observed permanent magnetism should be the same as that observed in thiol-capped gold nanoparticles.[6b] The hysteretic behavior should not be due to the occurrence of a long-range interparticle magnetic order, but to an effective blocking of anisotropic magnetic moments, as suggested by the ZFC/FC curves that show the characteristics of the transition, with decreasing temperature, from the superparamagnetic to the blocked state of nanoparticle moments. Whereas in such a state particle moments are oriented along their randomly distributed anisotropy axes, in this case, the anisotropy involved is not that of single domain particles, but that due to surface Ag atoms bonded to S atoms of the dithiol groups. The Ag−S bond gives rise to a localized charge transfer from Ag to S atoms, originating from localized magnetic moments. Their large anisotropy, responsible for the ferromagnetic-like characteristics, results from the combination of the spin−orbit coupling and the breaking of lattice symmetry at the surface with respect to the Ag atoms in the particle core. Surface Ag atoms are involved in both Ag−Ag and Ag−S types of bonding and this determines the lack of spherical symmetry of the neighbor electric charge distribution.[8] Similar arguments, high spin−orbit coupling, and lack of spherical symmetry and consequent reduction of the quenching of the orbital moment, have been proposed by Gambardella et al. to account for the giant magnetic anisotropy in isolated Co atoms and Co chains deposited onto Pt substrates.[25] The similarity to the blocking process of particle moments exhibited by the ZFC/FC magnetization curves suggests the presence of long range interactions between localized moments within the Ag particle.

The anisotropy constant value can be deduced from the Arrhenius law within the Néel-Brown model for the superparamagnetic relaxation time, $K_a = 25K_bT_b/V$.[26a,b] T_b corresponds to the temperature at which the relaxation time of the particle moment is of the order of the experimental time window (about 100 s for macroscopic magnetic measurements); V is the particle volume; K_b is the Boltzmann constant. Taking for V the mean particle volume $\langle V \rangle$ and for T_b, 300 K, as some moments are still blocked at this temperature, it turns out that for sample S1, $K_a \geq 9 \times 10^6$ J/m^3 (comparable values are obtained for the S2 and S3 samples). Actually, as the magnetic moments are located only at the particle surface, the effective volume is much smaller than the particle volume. This would imply an even larger value of K_a. This value differs by an order of magnitude from the K_a value (7×10^7 J/m^3) reported and calculated in the same manner for gold particles of 1.4 nm mean diameter capped by dodecanethiol,[6b] for which higher coercive fields and a higher moment per surface atom were found (0.036 μ_B). Such differences are understandable considering two facts: (i) the strength of the spin−orbit coupling for gold (1.5 eV) is higher than that for silver (0.1 eV); (ii) the length of the carbon chain is twice as long in the capped gold particles (dodecane) than in the silver ones (hexane), making the charge-transfer more effective. Indeed, as reported in the literature, the charge transfer from a metal to the thiol increases by increasing the carbon chain length.[9a,10]

Conclusions

Oleic acid-capped silver nanoparticles and 1,6-hexanedithiol-capped silver nanoparticles, synthesized by the polyol method, were structurally and morphologically characterized by XRD, STM, and TEM measurements and their electronic and magnetic properties were investigated by UV−visible and magnetization measurements, respectively. Unlike oleic acid-capped silver particles with diamagnetic behavior, the dithiol-capped silver particles exhibit permanent magnetism up to room temperature, as shown by hysteresis loops with finite coercivity. The temperature dependence of the low field magnetization, exhibiting features similar to those of a progressive blocking of nanoparticle moments, suggests that the observed permanent magnetism is due to magnetic moments blocked because of their high magnetic anisotropy. They are associated with silver atoms at the particle surface and are due to localized extra holes induced in the 4d band by the dithiol ligand through the Ag−S bonds. The large magnetic anisotropy of the localized moments results from

(25) Gambardella, P.; Rusponi, S.; Veronese, M.; Dhesi, S. S.; Grazioli, C.; Dallmeyer, A.; Cabria, I.; Zeller, R.; Dederichs, P. H.; Kern, K.; Carbone, C.; Brune, H. *Science* **2003**, *300*, 1130.
(26) (a) Neel, L. *Ann. Geophys.* **1949**, *5*, 99. (b) Brown, W. F. *Phys. Rev.* **1963**, *130*, 1677.

the combination of the Ag spin−orbit coupling and the lack of spherical symmetry of the surface Ag atoms bonded to Ag and dithiol-S atoms. This is the first time, as far as we know, that permanent magnetism has been observed in functionalized silver nanoparticles.

Acknowledgment. We wish to thank Dr. N. Domingo and Dr. M. Vasquez for help with magnetic measurements and Mr. P. Filaci for technical assistance.

CM062093A